JGR Biogeosciences

RESEARCH ARTICLE
10.1029/2023JG007630

Empirical Dynamic Modeling Reveals Complexity of Methane Fluxes in a Temperate Salt Marsh

Andrew C. Hill[1,2], Karina V. R. Schäfer[3], Inke Forbrich[4,5], and Rodrigo Vargas[1]

[1]Department of Plant & Soil Sciences, University of Delaware, Newark, DE, USA, [2]Northern Research Station, United States Forest Service, Grand Rapids, MN, USA, [3]Department of Earth and Environmental Sciences, Rutgers University, Newark, NJ, USA, [4]Marine Biological Laboratory, The Ecosystems Center, Woods Hole, MA, USA, [5]Department of Environmental Sciences, University of Toledo, Toledo, OH, USA

Key Points:

- Methane dynamics in salt marshes are complex and influenced by multiple variables
- Empirical dynamic modeling and convergent cross mapping are novel approaches to characterizing CH_4 dynamics
- Results highlight drivers, non-linearities, lag times, and interconnections among multiple biophysical variables for CH_4 dynamics

Supporting Information:

Supporting Information may be found in the online version of this article.

Correspondence to:

R. Vargas,
rvargas@udel.edu

Citation:

Hill, A. C., Schäfer, K. V. R., Forbrich, I., & Vargas, R. (2024). Empirical dynamic modeling reveals complexity of methane fluxes in a temperate salt marsh. *Journal of Geophysical Research: Biogeosciences*, *129*, e2023JG007630. https://doi.org/10.1029/2023JG007630

Received 12 JUN 2023
Accepted 2 FEB 2024

Abstract Methane dynamics within salt marshes are complex because vegetation types, temperature, oscillating water levels, and changes in salinity and redox conditions influence CH_4 production, consumption, oxidation, and emissions. These non-linear and complex interactions among variables affect the traditionally expected functional relationships and present challenges for interpreting and developing process-based models. We employed empirical dynamic modeling (EDM) and convergent cross mapping (CCM) as a novel approach for characterizing seasonal/multiday and diurnal CH_4 dynamics by inferring causal variables, lags, and interconnections among multiple biophysical variables within a temperate salt marsh using 5 years of eddy covariance data. EDM/CCM is a nonparametric approach capable of quantifying the coupling between variables while determining time scales where variable interactions are the most relevant. We found that gross primary productivity, tidal creek dissolved oxygen, and temperature were important for seasonal/multiday dynamics (rho = 0.73–0.80), while water level was most important for diurnal dynamics during both the growing and dormancy phenoperiods (rho = 0.72 and 0.56, respectively). Lags for the top-ranked variables (i.e., gross primary productivity, dissolved oxygen, temperature, water level) occurred between 1 and 5 weeks at the seasonal scale and 1–24 hr at the diurnal scale. The EDM had high prediction capabilities for intra-/inter-seasonal patterns and annual CH_4 sums but had limitations in representing large, infrequent fluxes. Results highlight the importance of non-linearity, drivers, lag times, and interconnections among multiple biophysical variables that regulate CH_4 fluxes in tidal wetlands. This research introduces a novel approach to examining CH_4 fluxes, which will aid in evaluating current paradigms in wetlands and other ecosystems.

Plain Language Summary The movement of methane gas in salt marshes is complex and influenced by various factors such as plant types, temperature, water level, and changes in water salinity and oxygen levels. These factors interact in complex ways, making predicting the outcome of methane production and movement difficult. We applied a new method of studying methane dynamics using Empirical Dynamic Modeling and Convergent Cross Mapping. After analyzing 5 years of ecosystem-scale measurements of methane fluxes, we show that the amount of oxygen in the water, the temperature, and the amount of light received by plants are crucial for understanding regulating methane fluxes within days and across seasons. The interconnections among these variables are complex, and methane fluxes may have delayed responses (i.e., lag times), highlighting the importance of these interactions. This research improves our comprehension of how environmental factors interact to affect methane fluxes in wetlands.

1. Introduction

Methane (CH_4) is the second most potent greenhouse gas and a crucial atmospheric trace gas with a warming potential 25–38 times greater than carbon dioxide (CO_2) (Bridgham et al., 2013; Neubauer & Megonigal, 2019; Wuebbles & Hayhoe, 2002). Following a largely unreconciled plateau during a stabilized phase from 2000 to 2006, there has been a steady global rise, with wetlands likely responsible for most natural contributions (Jackson et al., 2020). While there is evidence that this increase is the result of both anthropogenic and biogenic emissions (Stavert et al., 2022), there is no easy mitigation option for biogenic sources, and climate change could increase these emissions resulting in a positive feedback for the global carbon cycle (Dean et al., 2018; Zhang et al., 2017). This is especially important for coastal wetlands where warming and sea level rise are expected to impact CH_4 fluxes directly through changes in microbial metabolism (Lu et al., 2018; Yvon-Durocher et al., 2014), and

indirectly from effects on co-dependent factors such as plant productivity (GPP) and sediment redox conditions (Liu et al., 2019; Seyfferth et al., 2020; Strom et al., 2015).

Mechanisms driving CH_4 fluxes are complex within coastal wetlands with many potential regulators (Huertas et al., 2019; Vázquez-Lule & Vargas, 2021) and pathways for production and efflux (Capooci et al., 2024). Water level and waterlogged conditions have been identified as a substantial control for methanogenesis in coastal wetlands (Li, 2007), but these ecosystems have been considered low CH_4 emitters despite prevailing anoxic conditions (Bartlett et al., 1987; Borges & Abril, 2011; Conrad, 2020). This paradigm relies on the idea that acetoclastic or hydrogenotrophic methanogenesis are the dominant biogeochemical pathways and prevailing sulfate-reducing bacteria outcompete methanogens (Poffenbarger et al., 2011). However, several lines of evidence indicate coastal wetlands could have high CH_4 fluxes where other biogeochemical pathways, such as methylotrophic methanogenesis, play essential roles (Al-Haj & Fulweiler, 2020; Capooci et al., 2024; Conrad, 2020; Oremland & Polcin, 1982; Seyfferth et al., 2020). In addition, it has been suggested that multiple environmental factors (e.g., water level, temperature, GPP, salinity) regulate CH_4 fluxes at different temporal scales with potential nonlinear interactions (Huertas et al., 2019; Reid et al., 2013). Consequently, it is imperative that we accurately understand how biophysical controls regulate CH_4 fluxes in coastal wetlands to understand ecosystem response to environmental change.

Our past knowledge of CH_4 dynamics in tidal wetlands has vastly relied on chamber-based manual measurements. This information has influenced the development of most functional relationships (e.g., salinity thresholds or temperature dependency) and, subsequently their incorporation into models used to predict CH_4 fluxes. However, chambers often face logistical challenges and are sporadic in time and space, restricting our understanding by delivering limited or incomplete information (Hill & Vargas, 2022; Kim, 2007; Yang et al., 2021) that could result in biased estimates of annual fluxes (Vargas & Le, 2023). Technological advances have allowed us to collect higher frequency CH_4 fluxes at the ecosystem scale using the eddy covariance technique (EC) (Baldocchi, 2003; Morin, 2019). This data can be leveraged to explore temporal relationships in greater detail, providing a wealth of information regarding the dynamics of driving mechanisms. Previous studies have analyzed how biophysical variables regulate ecosystem-scale CH_4 fluxes in salt marshes (Hill & Vargas, 2022; Huertas et al., 2019; Reid et al., 2013; Vázquez-Lule & Vargas, 2021). Other studies outside salt marshes have used machine learning techniques (Rey-Sanchez et al., 2018; Zaki & Abdul-Aziz, 2022) or time series analysis and information theory to identify the dominant controls of ecosystem-scale CH_4 fluxes (Knox et al., 2021; Sturtevant et al., 2016). Together, these studies provide insights into the complex mechanisms and hint that nonlinear dynamics may be more relevant for explaining ecosystem-scale CH_4 fluxes. Therefore, there is a need to identify potential lags, interactions, and interconnections to provide insights about causality and biogeochemical mechanisms controlling CH_4 fluxes across wetland types.

The complexity of CH_4 dynamics in coastal wetlands results from interacting variables that cannot be readily isolated to identify independent functional relationships (Morin, 2019; Vázquez-Lule & Vargas, 2021). As a novel approach, we employed a form of nonlinear state space reconstruction referred to as empirical dynamic modeling (EDM) which operates in the state space as opposed to observational space (Park & Stabenau, 2022; Sugihara & May, 1990; Sugihara et al., 2012). Specifically, we used convergent cross mapping (CCM) as a novel approach to disentangling CH_4 drivers within a temperate salt marsh and a multivariate EDM model to predict CH_4 fluxes (Munch et al., 2023). We propose EDM as an alternative to techniques such as Granger Causality, wavelet analysis, and information theory to unravel complex non-linear CH_4 dynamics (Knox et al., 2021; Schafer et al., 2014; Sturtevant et al., 2016; Vargas et al., 2010).

The premise of EDM relies upon a simplex algorithm that projects observed time series into an *e*-multidimensional state space. The value of *e* (embedding dimension) is determined before performing CCM or any modeling. In CCM, two time series (e.g., X_t and Y_t) are projected into their respective *e*-dimensional state spaces (e.g., X_s and Y_s) and values of Y_s are used to make nearest neighbor predictions about X_s (cross-mapping) and vice versa (reverse cross-mapping). Information content between the two projections is evaluated with the parameter rho (ρ) at maximum sample size, which is similar to Pearson's correlation coefficient but determined within state space. To infer causality, we expect rho to increase with increasing sample size (i.e., convergence) in the direction of the best cross-mapping (i.e., does X cause Y or Y cause X). Then, the target time series is split for analysis in a multivariate model, and a nearest neighbor forecasting method is used to track the evolution of nearby points within the projected multivariate state space (Hsieh et al., 2005). Finally, points are predicted forward in time for

the out-of-sample portion of the time series as a validation method. We chose the EDM because it can describe complex interrelations, infer causality, and make predictions in a dynamic ecological system where variables cannot be evaluated independently.

Here, we examine primary data from 5 years of ecosystem-scale CH_4 fluxes using the EC technique and EDM to study seasonal and diurnal CH_4 fluxes (i.e., dependent variable) by quantifying the coupling between independent variables (i.e., predictors) while considering time lags and interconnections. We first use CCM to infer causal relationships between a suite of ancillary variables and CH_4 fluxes. For variables that indicate a causal link, we then apply the analysis at a range of time periods to identify relevant time lags or synchronies. We also test all relevant pairs of ancillary variables with CCM to elucidate complex interactions using causal network maps. Finally, we construct a multivariate EDM model using the inferred causal variables to make out-of-sample predictions. EDM and CCM have been used in a variety of ecological studies (Chang et al., 2017; Deyle et al., 2016; Munch et al., 2018; Sugihara et al., 2012), but have not yet been applied for analyzing eddy covariance data. Because CH_4 dynamics exhibit complex patterns generated by multiple interactions, we propose that EDM is best suited to identify the nonlinearities and potential causal relationships that regulate CH_4 dynamics in wetlands and other terrestrial ecosystems.

2. Materials and Methods

2.1. Study Site

This study was performed at the St. Jones Reserve as part of the Delaware National Estuarine Research Reserve System (DNERR). The site is representative of a natural, unrestored mid-Atlantic salt marsh that receives drainage from highly developed inland areas with a mean elevation of 0.60 ± 0.26 m relative to the NAVD88 datum (McKenna et al., 2018), yet is still influenced by semi-diurnal tidal activity and site hydrology (i.e., riverine and groundwater flows). Vegetation is dominated by a monoculture of short-form *S. alterniflora* (~66%). The remaining cover (~33%) is associated with tall *S. alterniflora*, *S. cynosuroides*, *and P. australis*, which flank tidal creeks, and *S. patens* and *P. australis* along the upland terminus (Vázquez-Lule & Vargas, 2021; Vázquez-Lule et al., 2022). The prevailing paradigm assumes that low methanogenesis is expected in these salt marshes, but recent studies have challenged it by demonstrating high rates of methanogenesis (particularly methylotrophic) at the study site (Capooci & Vargas, 2022; Capooci et al., 2019, 2024; Seyferth et al., 2020). Therefore, new approaches are needed to identify the complexity of the underlying biophysical drivers of CH_4 fluxes.

2.2. Data Acquisition

2.2.1. Eddy Covariance Measurements

The eddy covariance (EC) technique was used to measure the ecosystem-scale net exchange of CH_4 with an open path near-infrared gas analyzer (Li-7700, Licor, Lincoln, NE, USA) and ecosystem-scale net exchange of CO_2 (NEE) with an enclosed path infrared gas analyzer (Li-7200, Licor, Lincoln, NE, USA), and wind components with a 3D sonic anemometer (Gill Windmaster Pro, Gill Instruments, Lymington, UK) recording measurements at 10 Hz. Preprocessing was completed in Eddy Pro (version 7.0.6), which consisted of time lag compensations, double coordinate rotation of wind components, and Reynolds block averaging to calculate 30-min fluxes of CH_4 and CO_2. Expanded preprocessing and tower set-up descriptions can be found elsewhere (Hill & Vargas, 2022; Vázquez-Lule & Vargas, 2021). During post-processing, several standardized Ameriflux QA/QC procedures were applied. These included removing values flagged for low quality during pre-processing, calculating nighttime storage fluxes determined by Eddy Pro, and range filtering of CO_2 to remove outliers falling beyond ±50 μmol m^{-2} s^{-1}, as these values are outside the typical NEE range observed at this site (Vázquez-Lule & Vargas, 2021). A range filter was not applied to CH_4 data as spikes due to ebullition could occur, and the goal was to incorporate all CH_4 dynamics within the 30-min block averaging period. In addition, we used an optimal friction velocity (u^*) threshold of 0.069 m s^{-1} to remove low turbulence conditions and applied a fetch/footprint filter to exclude fluxes originating from forested regions beyond the marsh terminus (Vázquez-Lule & Vargas, 2021; Vazquez-Lule et al., 2022).

Data gaps occurring in NEE were filled using marginal distribution sampling (MDS) with customized site variables consisting of energy fluxes (sensible and latent heat; H and LE), radiation, air temperature (Tair), soil temperature (Tsoil), relative humidity (RH) and vapor pressure deficit (VPD) (Vázquez-Lule & Vargas, 2021).

Table 1
Definition List for All Variables Used in the Study

Variable	Abbreviation	Units
Air Temperature	Tair	°C
Atmospheric Pressure	BP	kPa
Carbon Dioxide (flux)	CO_2, NEE	umol m^{-2} s^{-1}
Dissolved Oxygen	DO	mg L^{-1}
Gross Primary Productivity	GPP	umol m^{-2} s^{-1}
Latent Heat Flux	LE	watts m^{-2} s^{-1}
Methane (flux)	CH_4	nmol m^{-2} s^{-1}
Photosynthetically Active Radiation	PAR	umol m^{-2} s^{-1}
Precipitation	Precip	mm
Relative Humidity	RH	%
Salinity	Sal	ppt
Sensible Heat (flux)	H	watts m^{-2} s^{-1}
Soil Temperature	Tsoil	°C
Vapor Pressure Deficit	VPD	kPa
Water Level	Level	m
Water Temperature	Twater	°C
Water Vapor (flux)	H_2O	mmol m^{-2} s^{-1}
Wind Speed	WSpd	m^{-2} s^{-1}

Partitioning of NEE into component fluxes of gross primary productivity (GPP) was completed with the REddyProc R package (Reichstein et al., 2005; Wutzler et al., 2018) based on the standard nighttime method (Reichstein et al., 2005). To fill gaps in CH_4 fluxes, we applied a random forest technique with the Caret R package and used a full suite of relevant site variables (Figure S1 in Supporting Information S1) (Kim et al., 2020; Kuhn, 2008). This method was selected because it is less biased when identifying predictors of CH_4 flux and, like other time series analyses (e.g., wavelets), CCM requires continuous gap-filled data. In many time series analyses, gaps are ignored in computations, in our case causing the lagged state space reconstructions to fail; therefore, gap filled data is commonly used (Chang et al., 2017; Dietze et al., 2011; Kim et al., 2020; Vargas et al., 2018).

2.2.2. Meteorology and Water Quality Measurements

Meteorological variables included air temperature (Tair), relative humidity (RH, HC2-S3, Campbell Scientific, Logan, UT), precipitation (Precip) (TE 525, Tipping Bucket Rain Gauge, Campbell Scientific, Logan, UT), photosynthetically active radiation (PAR) (SQ-110, quantum sensor, Apogee, Logan, UT), air pressure (Patm) (CS-106, Vaisala, Vantaa, Finland) and wind speed (WSpd) (05103-L Wind Monitor, Campbell Scientific, Logan, UT). VPD was calculated using Tair and RH based on the Tetens formula (Murray, 1967). Water quality data were collected from the tidal creek adjacent to the EC tower using a YSI EXO2 sonde outfitted with EXO sensors. Measured variables included water temperature (Twater), water level (Level), salinity (Sal), and dissolved oxygen (DO). Meteorological and water quality data were averaged for 30 min to align with flux data. Minor gaps in meteorological data were filled using available on-site sensors. Gaps in water quality data, mainly during the dormancy phenoperiod (<20% of the data), were filled using empirical relationships from another YSI EXO2 sonde located approximately 2 km upstream within the St. Jones River, which shares connectivity to the tidal channel. Despite the potential limitations of inferring these values, the overall relationships were significant and positive. Thus, this approach should not impact the conclusions of the study. Meteorological and water quality data were collected under the National Estuarine Research Reserve (NERR) Centralized Data Management Protocol (Kennish, 2019) and can be accessed from the NERR System Centralized Data Management Office (NERR CDMO; station: delsjmet-p). All variables, their abbreviations, and units have been summarized in Table 1.

2.3. Data Selection and Phenology

For examining seasonal CH_4 dynamics, we selected five years spanning 2017–2021 to calculate daily means of non-gap-filled observations. This period was chosen as all years contained minimal continuous gaps (<30 days). The original half-hourly time series of post-processed CH_4 fluxes had 38% gaps. To examine diurnal dynamics, we used data only from 2020 to 2021, the period with the most complete record (i.e., containing 15% of data gaps) and when no substantial water surges or storm events occurred. To delineate growing and dormancy periods, we determined phenology dates with the Phenopix R package using the greenness chromatic coordinate (GCC) from a site phenocam (Filippa et al., 2016; Hill et al., 2021; Vázquez-Lule & Vargas, 2023). Season start and end dates were calculated based on the upturn and recession dates of the annual GCC curve from daily midday images (Gu et al., 2009). To avoid an artifact of calendar years that would result in discontinuous time series for dormancy data, we included the tail end of 2020 and excluded the tail end of 2021 (Dormancy: November 2020–April 2021, Growing: April 2021–October 2021).

2.4. Convergent Cross Mapping

While previous studies have described in detail the methodology behind CCM (Chang et al., 2017; Sugihara et al., 2012; Sugihara & May, 1990; Tsonis et al., 2018; Ushio & Kawatsu, 2020; Wang et al., 2018), we provide a brief overview of the implementation of CCM and how we interpreted results as they pertain to our objectives (Figure S2 in Supporting Information S1). We point out that while CCM is a powerful tool, results are based on

empirical methods; thus, interpretation of potential causalities should be interpreted with this in mind. All CCM analyses were completed within the rEDM R package (Ye et al., 2016).

To evaluate the causality between variables, we applied traditional bivariate CCM between CH_4 and all independent variables via the function CCM (Ye et al., 2016). The CCM function is essentially a wrapper for the simplex algorithm but accesses the level improvement in nearest neighbor predictions within the state space as the data sample size increases. Specifically, it tests if lags of a predictor variable can be used to predict a target variable (e.g., does GPP have a causal relationship with CH_4) (Schiecke et al., 2015; Sugihara et al., 2012; Tsonis et al., 2018). It is a standard procedure also to test the opposite cross mapping (i.e., does CH_4 have a causal relationship with GPP). In a dynamic system, information about the causal variable becomes embedded within the target variable (i.e., information about past causal variables is observed in the present target variable). CCM is carried out using successively larger time-ordered data chunks subsampled randomly from the main data set. For each of these CCM runs, the cross-mapping performance is evaluated with the output parameter rho (cross-mapping predictive skill). There is evidence of causality if rho is found to successively increase with larger data subsamples (i.e., convergence) (Chang et al., 2017). As a final step and significance test, the predictive skill generated at maximum library size (full data set) is compared to rho generated at maximum library size with a surrogate data set constructed from the original data randomized in time and containing a preserved seasonal phase amplitude (Tsonis et al., 2018).

Two steps are applied before CCM, which provide information about the time series of interest (CH_4) (Li et al., 2021). The initial step is determining the embedding dimension (e) via the function *EmbedDimension*, which iteratively takes successively longer lags of a set time period defined by the parameter Tau (T). For this study, we set T to the default value of $T = 1$ to represent one day for seasonal analyses and 1 hour for diurnal analyses. The lagged time series are then projected into an e-dimensional state space, forming a shadow manifold or state space projection (Ye et al., 2016) (Figure S3 in Supporting Information S1). The resulting manifolds are projected back onto a coordinate axis with the best embedding dimension resulting in a nearly 1:1 mapping of the original time series (Figure S4 in Supporting Information S1). The number of dimensions (e) required to recreate the original time series is both a metric of complexity and an a priori requirement for CCM. The second step is confirming nonlinear dynamics by constructing sequential locally weighted global linear maps (S-map). S-maps are like nearest neighbor predictions from the simplex algorithm, but instead of considering the average localization of the nearest neighbors, all neighboring points are regarded with more weight given to closer neighbors through an exponential localization function (Sugihara, 1994). This is done via the function *PredictNonlinear*, which determines if predictions made by S-maps display state or time dependence (i.e., relationships vary with time) as defined by the parameter theta (Θ) in a locally weighted linear regression function. If predictive skill increases at $\Theta > 0$, we assume that predictions are highly dependent on ecosystem state space (i.e., variable interactions change with time or under specific conditions) and the hallmark of a nonlinear dynamical system (Chang et al., 2017).

We applied year-round daily data for seasonal dynamics with a minimum sample size of $n = 15$ days and a maximum of $n = 1{,}800$ days. For diurnal dynamics, hourly data was used from the selected growing and dormancy phenoperiods using a minimum sample size of $n = 15$ hr and a maximum of $n = 2{,}900$ and $n = 2{,}700$ hr, respectively. Minimum sample sizes were selected to capture spring neap tidal cycles and sub-daily oscillations, while maximum sample sizes were selected to cover most of the selected time series. CCM was carried out using sample runs with the default time period for lags set to 1 unit (Tp = 1 day or hour). The execution radius, which ignores nearest neighbors within the state space projection, was set at one day or 24 hr to help eliminate influence from temporal autocorrelation. To generate surrogate data sets, the original data was randomized in time with the seasonal phase amplitude preserved for daily data by setting the method to "seasonal." For hourly data, the method was set to "random" (Deyle et al., 2016).

2.5. Model Interpretation With Extended CCM and Causal Network Maps

Conventional CCM provides a robust means of identifying causality between variable pairs, yet it fails to capture the optimal time period of the causal influence. Extended CCM is a computationally intensive technique that involves applying CCM iteratively across multiple time period lags to determine time periods where cross-mapping skills are maximized. The procedure is also used to help resolve issues of generalized synchrony where cross-mapping is significant in both directions (i.e., Tair causality on CH_4 and CH_4 causality on Tair) as the

most probable causal relationship will generally have a maximum predictive skill which peaks within the negative time domain (i.e., negative lags), while the reverse cross-mapping peaks in the positive time domain (i.e., positive lags; Ye et al., 2015). Variable interactions can occur synchronously, over a day, several hours, or several consecutive or separate days (Sun et al., 2021). Data were binned into 7-day periods to examine seasonal dynamics, and iterations were made spanning ±91 days at weekly intervals. For diurnal dynamics, hourly data was used directly, and iterations were made spanning ±24 hr.

We constructed causal network maps based on the bivariate CCM results, to assess how the identified drivers interact to influence CH_4 fluxes (Fan et al., 2020; Ye et al., 2016). Conceptually, this is achieved by summarizing the strength of coupling between all tested variable pairs (Ye et al., 2015), including all ancillary variables with only positively identified (significant) connections mapped. Here, we selected ranking categories of high, moderate, and low based on rho values of 0.60–1.0, 0.30–0.59, and 0–0.29, respectively (Fan et al., 2020). We focus on drivers controlling CH_4 fluxes as "direct" drivers, while drivers controlling other variables in the system (e.g., GPP) are defined as "indirect" drivers. This technique allows variables with indirect links that may appear to influence CH_4 fluxes to be sorted from those with highly confident direct causal links. However, it is challenging to distinguish the consistent directionality (i.e., positive or negative sign) of the connection because relationships can vary over time (i.e., state dependence). Thus, this analysis defines the overall importance of each causal variable, as explained in other studies (Deyle et al., 2016).

2.6. Multivariate Predictive Modeling

We performed model predictions using a newly constructed multivariate EDM model as an additional feature and promising application of EDM. We used an out-of-sample validation method with data from 2017 to 2019 as the training interval and data from 2020 to 2021 as the prediction interval. We included only non-gap-filled data for the performance comparisons. Predictor data were scaled to reduce dimensional distortion in the state space. The provided prediction variance based on nearest neighbors in the state space was used to calculate the standard deviation as a metric of uncertainty. We included all variables identified as being coupled with CH_4 fluxes by daily CCM analysis: temperature components of soil, water, and air, DO, GPP, H_2O flux, Level, LE, WSpd, PAR, Patm, RH, and Precip. While issues of cross-correlation could potentially violate assumptions for linear models, each of these variables interacts with CH_4 fluxes in different ways as determined by the information embedded in the CH_4 time series. Thus, including variables that exhibit cross-correlation with linear evaluation methods is possible with EDM.

3. Results

3.1. Site Characteristics, Phenology, and CH_4 Fluxes

During the study period (2017–2021), the annual average air temperature (Tair), salinity (Sal), and water level (Level) were 13.9 ± 9.1°C, 8.9 ± 4.1 ppt and 0.25 ± 0.2 m above sea level, respectively with a tidal range of 1.2 m and maximum daily salinity as high as 19.5 ppt. The average annual precipitation (Precip) ranged from 567 to 779 mm, which is received evenly across the year (Figure 1) (Tables S1–S3 in Supporting Information S1). The growing phenoperiod typically begins with green-up events occurring in April or early May, and dormancy commences with complete vegetation senescence in November. For the reference year utilizing hourly data (2020–2021), the dormancy phenoperiod began on October 25. It ended at the start of the 2021 growing phenoperiod on April 26, which continued until the subsequent dormancy phenoperiod on October 23. Despite high levels of GPP, which ranged from 1,412–1,609 g C m^{-2} yr^{-1}, the site was a net carbon source for four out of the five years (NEE range: −126 to 221 g C m^{-2} yr^{-1}) and was a constant annual source of CH_4 with emissions ranging from 15.4 to 16.5 g C m^{-2} yr^{-1} (Figure 1).

3.2. CH_4 Time Series Characteristics

We determined that CH_4 is a highly dimensional independent variable that required at least 10 dimensions to recreate the original dynamics (Figure S5 in Supporting Information S1). Despite a slightly lower peak at four dimensions, we selected the dimensionality with the greatest predictive skill to capture a full range of potential variable dynamics; because CCM is expected to identify coupling and quantify the overall strength of all possible relationships. This indicates that the response of CH_4 flux was highly dependent on state space or transient ecosystem conditions (i.e., dynamical, and nonlinear) (Figure S6 in Supporting Information S1).

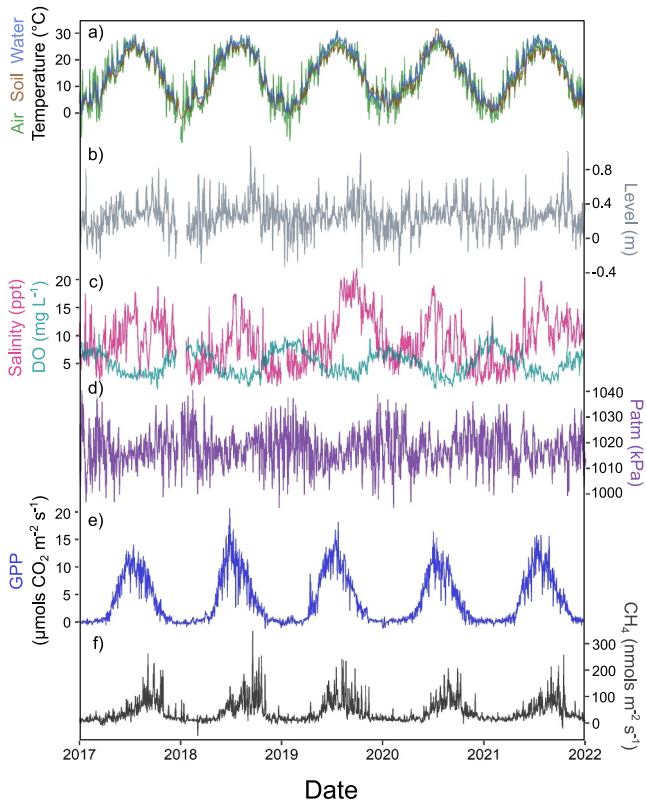

Figure 1. Time series of mean daily data for top identified predictive variables and CH_4 flux from 2017 to 2021. (a) Air, soil, and water temperature (green, brown, and blue, respectively), (b) level (gray), (c) and (d) salinity (pink) and dissolved oxygen (DO) (teal), (d) atmospheric pressure (Patm) (purple), (e) gross primary productivity (GPP) (blue), and (f) CH_4 flux (black).

3.3. Causality Analysis With CCM

Examination of daily data with CCM at the seasonal/multiday scale identified temperature components (Tsoil, Twater, Tair), DO, and GPP (Figure 2a) as important variables. These variables were a distinct grouping, with all other variables falling below a threshold of rho = 0.50. The remaining variables (H_2O flux, Level, LE, PAR, WSpd, Patm, RH, Precip; sorted from higher to lower coupling strength) were identified as important (rho = 0.10–0.50) except for Sal, VPD, and H, which did not meet the convergence criteria or overlapped with surrogate data (Figure S7 in Supporting Information S1). The growing phenoperiod was complex regarding the number of predictors and lags, yet physical factors also likely played an important role. Examination of hourly data for the diel scale analysis from the growing phenoperiod identified Level as the most important variable (rho ~ 0.70), followed by a grouping that included Patm, Sal, DO, and Tsoil (rho = 0.30–0.50) (Figure 3a). The remaining variables (PAR, Twater, RH, GPP, H, H_2O flux, WSpd, LE, VPD, Tair; sorted from higher to lower coupling strength) also had a degree of coupling (rho = 0.15–0.25), except for Precip (Figure S8 in Supporting Information S1). Examination of hourly data from the dormancy phenoperiod identified Level, DO, and Sal as important variables (rho = 0.55–0.30) (Figure 3c). Most remaining variables (Patm, RH, WSpd, Tair, VPD, PAR, Precip; sorted from higher to lower coupling strength) also exhibited some coupling (rho = 0.10–0.20), yet this period contained the largest number of non-significant variables, which included GPP, Tsoil, Twater, H, LE, and water fluxes (Figure S9 in Supporting Information S1).

3.4. Optimal Lags With Extended CCM

Implementation of extended CCM indicated that the influence of some variables is likely more immediate while others are associated with a lag. While any identified lags indicate the optimal time period of influence, these lags are not necessarily related to the overall strength of the relationship. However, longer lags can mean more indirect relationships within the context of causal network mapping (Fan et al., 2020). When applying daily data to unravel seasonal/multiday dynamics of CH_4 fluxes, we found that PAR, LE, and H_2O fluxes are associated with the most extended lag times occurring between 49 and 70 days (seasonal/multiday scale) (moderate importance). These were followed by a grouping of top predictor variables identified by the previous CCM analysis (Tsoil, Twater, Tair, GPP) (high importance), which were identified as most influential between 21 and 35 days (monthly scale). The remaining variables (DO, Level, WSpd, Patm, RH, Precip) exerted a close temporal relationship (0 days) at a range of strengths but DO was important over a more extended period (0–3 weeks), followed by Level, Patm, and RH (0–1 week) and finally WSpd and Precip (0 days). However, Precip had the weakest coupling (Figure 2b) (Figure S10 in Supporting Information S1).

When applying hourly data from the growing phenoperiod to unravel diurnal dynamics, we found that lags were more complex. Both Level and Sal (strong and moderate importance, respectively) had peaks occurring between 0 and 5 hr and again between 19 and 23 hr, but the influence of Level was also persistent throughout the day (denoted as a gray bar in Figure 3b). Temperature components had successively shorter lags moving from Twater (9–13 hr) to Tsoil (5–7 hr) and finally Tair (3–6 hr) (all moderate causal strength). The remaining variables were influential immediately (0 hr), with GPP extending the longest (0–9 hr), followed by Patm (0–5 hr), LE and water fluxes (0–3 hr), RH (0–1 hr) and finally DO, VPD, and H (0 hr) (moderate causal strength) (Figure 3b) (Figure S11 in Supporting Information S1). Lag times were much shorter for the dormancy phenoperiod. Almost all variables identified as important (Level, DO, Sal, Patm, RH, Tair, VPD, Tsoil) exerted a close temporal relationship (0 hr) with DO, VPD, Tsoil, Patm, and Level active over the most extended period (0–10 hr). Precip was influential between 7 and 8 hr, yet again had the lowest importance while PAR, RH, WSpd, and Tair all exerted influence between 0 and 5 hr (moderate importance strength) (Figure 3d) (Figure S12 in Supporting Information S1).

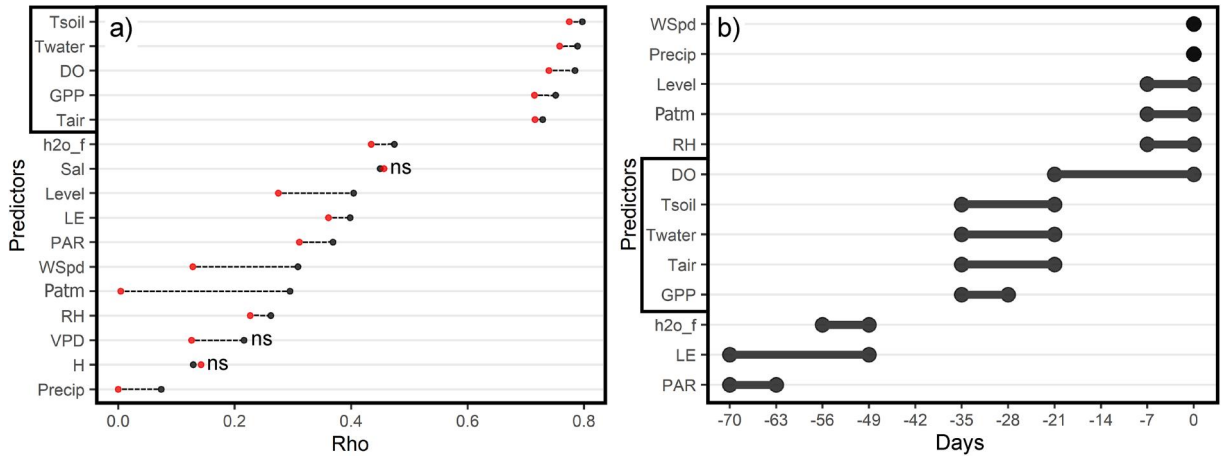

Figure 2. Results from Convergent cross mapping (CCM) and extended CCM for seasonal dynamics from daily data spanning 2017–2021. (a) Identification of strongest predictor variables for CH_4 flux using CCM. Red points represent the maximum predictive skill achieved using the simulated surrogate data. Black points indicate prediction skill of training data. *ns* denotes non-significant cross-mapping owing to a lack of convergence or overlap with the surrogate data results. Outlined variables exhibited a prediction skill >0.6. (b) Optimal time lags (in number of days) determined using the extended CCM. See Table 1 for a list of variable definitions.

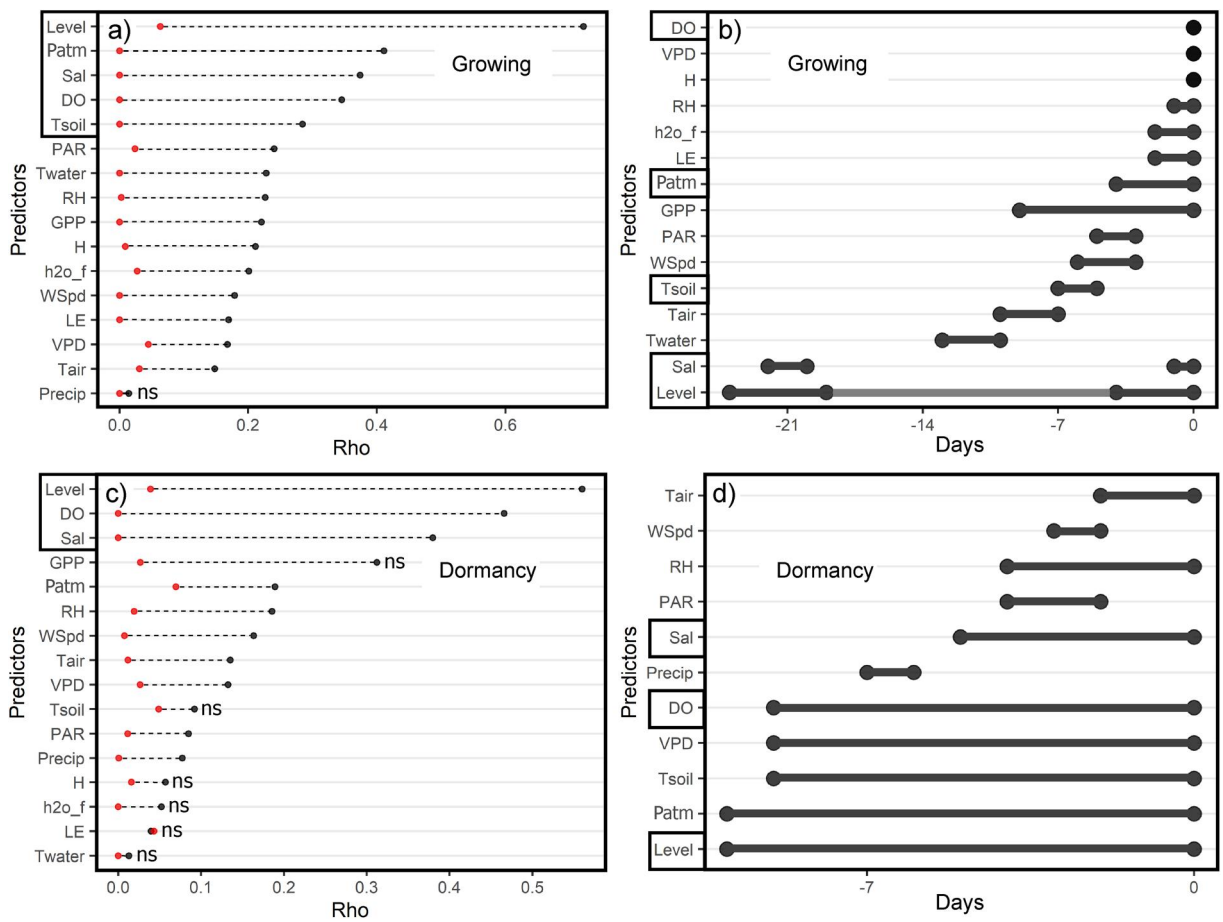

Figure 3. Results from Convergent cross mapping (CCM) and extended CCM for diurnal/seasonal dynamics from selected hourly data spanning years 2020–2021. (a) Growing phenoperiod CCM at maximum library size between all variables and CH_4 flux, (b) Growing phenoperiod optimal time lags (in number of days) for extended, (c) Dormancy phenoperiod CCM at maximum library size between all variables and CH_4 flux. (d) Dormancy phenoperiod optimal time lags (in number of days) for extended CCM. Red points represent the maximum predictive skill achieved with simulated surrogate data. Black points indicate the prediction skill of training data. *ns* denotes non-significant cross-mapping due to a lack of convergence or overlap with surrogate results. Outlined variables exhibit a prediction skill >0.3. See Table 1 for a list of variable definitions.

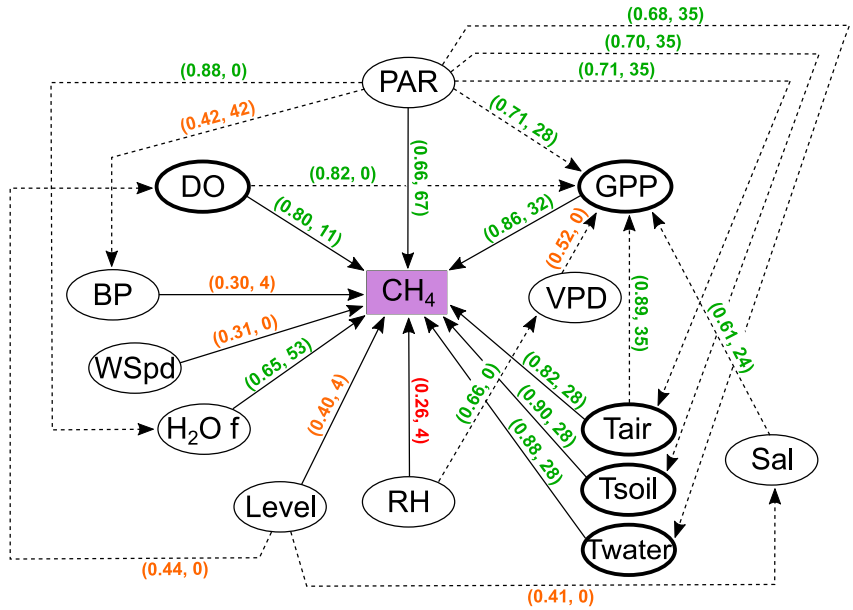

Figure 4. Causal network map showing seasonal dynamics between all relevant variables for daily data spanning 2017–2021. Numbers represent predictive skill followed by the median value of the optimum time lag (days). Colors represent the strength of coupling, green = strong (0.6–1.0), orange = moderate (0.30–0.59), and red (weak) (0–0.29). Solid lines represent significant relationships with CH_4, and dashed lines represent significant relationships between ancillary variables. Variables outlined in bold represent the top causal variables identified by CCM analysis. See Table 1 for a list of variable definitions.

3.5. Causal Network Mapping

Causal network maps show high interconnection among variables at multiple scales (seasonal, multiday, and diurnal) and indicate that fluxes result from a suite of factors. When using daily data, we discovered several interesting patterns (Figure 4). First, PAR is important for CH_4 (rho = 0.66), but its influence may be tied to other relevant variables (e.g., H_2O fluxes and temperature components) (rho = 0.68–0.88). The strong relationship between GPP and CH_4 fluxes (rho = 0.86) was influenced by VPD, Tair, Sal, and DO (rho = 0.52–0.82), which are in turn influenced by RH, PAR, and Level, respectively (rho = 0.41–0.71). Other variables, such as RH and WSpd, were not connected to any variables examined.

When applying hourly data for the growing phenoperiod, many highly connected variables identified from the seasonal analysis (Temperature components, GPP, DO) exert far less influence (Figure 5a). The water level was the most directly important variable (rho = 0.72) and was highly connected to both Sal and DO (rho-0.90-92), which exerted moderate influence on CH_4 fluxes (rho = 0.35–0.38). Over seven additional variables provided moderate-low influence, but all showed a similar predictive skill (rho = 0.17–0.41), highlighting the complexity associated with the sub-daily growing phenoperiod. Hourly data from the dormancy phenoperiod exhibited the most straightforward network connectivity with the least interdependencies (Figure 5b). As with growing phenoperiod data, Level was identified as an important variable (rho = 0.60) and exerted a strong influence on Sal and DO (rho = 0.81–89), which exerted moderate influence on CH_4 fluxes (rho = 0.38–0.49). Additional variables were associated with weaker relationships (rho = 0.12–0.22), and only temperature components, VPD, Patm, Sal, and DO were dependent on the activity of other variables during this phenoperiod.

3.6. Modeling Output

The predictive multivariate EDM model captured the changing seasonal dynamics well yet had difficulty predicting periodic emissions peaks, especially during fall senescence (Figures 6a and 6b). This model incorporated all of the positively coupled variables identified by CCM analysis, including temperature components of soil, water, air, GPP, DO, H_2O flux, Level, LE, PAR, WSpd, Patm, RH, and Precip. This generated a 2-year sum of 31.8 g C m^{-2} with an annual uncertainty of ±29.3 g C m^{-2}, calculated from the state space. Despite good overall

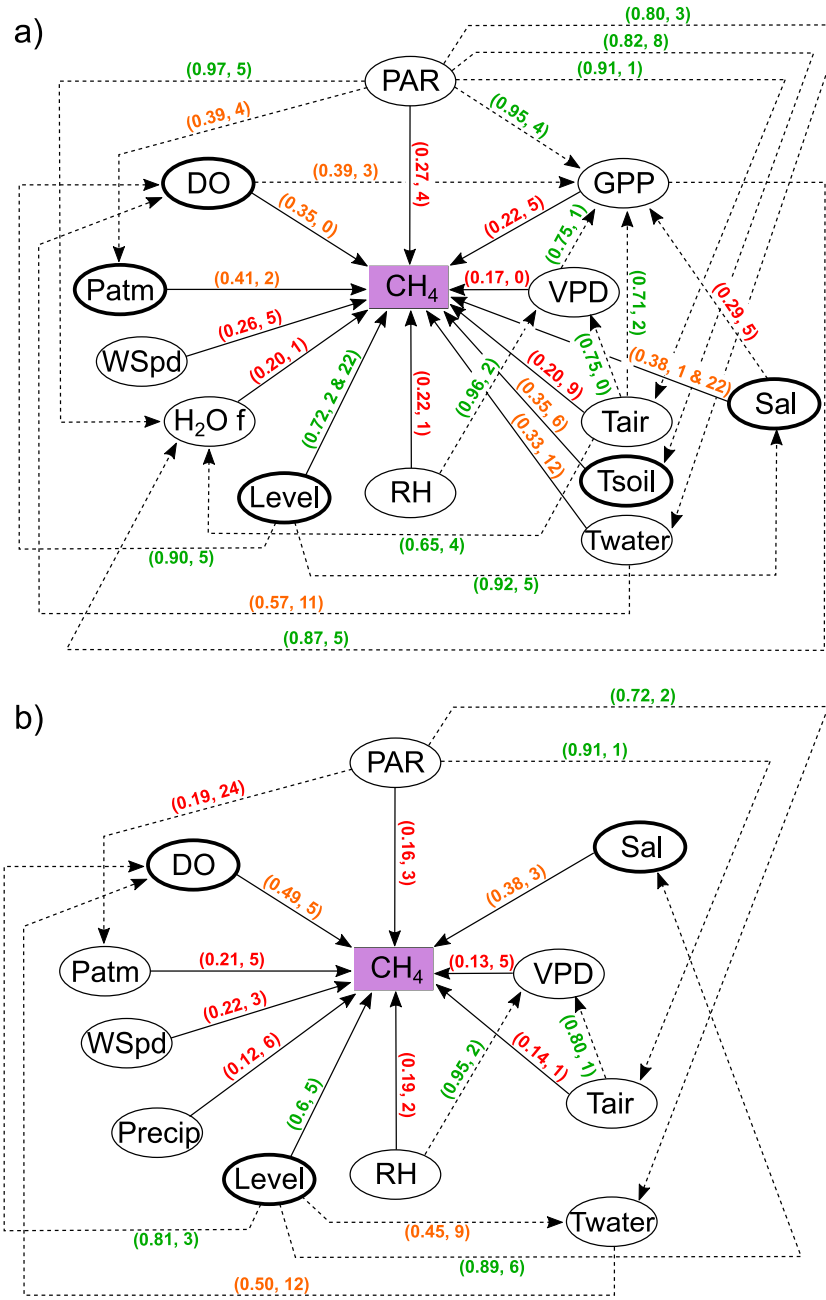

Figure 5. Causal network maps showing diurnal/seasonal dynamics between all relevant variables for select hourly data spanning 2020–2021 for (a) Growing phenoperiod and (b) Dormancy phenoperiod. Numbers represent predictive skill followed by the median value of the optimum time lag (hours). Colors represent the strength of coupling, green = strong (0.6–1.0), orange = moderate (0.30–0.59), and red (weak) (0–0.29). Solid lines represent significant relationships with CH_4, and dashed lines represent significant relationships between ancillary variables. Variables outlined in bold represent the top ranked variables identified by CCM analysis. See Table 1 for a list of variable definitions.

predictions, the approach had challenges representing high fluxes during senescence. There was higher uncertainty, small over-prediction bias for lower magnitude fluxes (<50 nmol m^{-2} s^{-1}), and an under-prediction bias for larger fluxes during senescence (Figure 6b). It is important to consider that the uncertainty estimate for the EDM model is derived from the nearest neighbor distance weights in the projected state space.

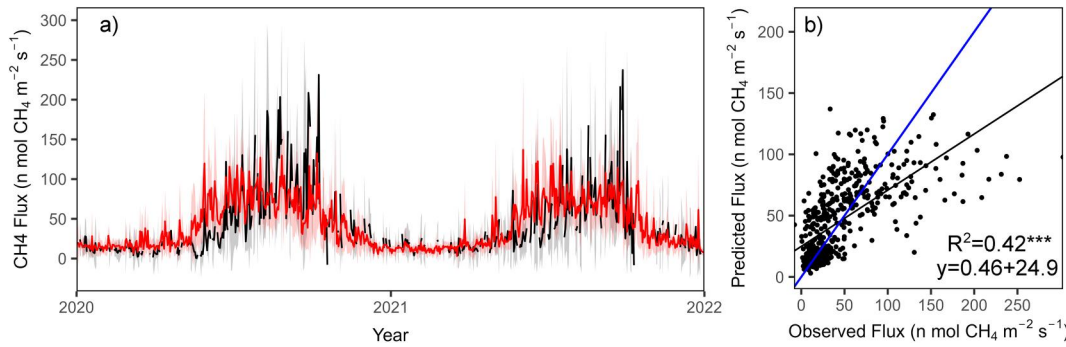

Figure 6. (a) Multivariate EDM modeling results at the daily time step for prediction years 2020–2021 and (b) linear regression comparisons. Black lines represent non-gap-filled daily CH_4 flux measured by eddy covariance (EC) as a benchmark ±daily sd (gray shading), and red lines represent daily modeled CH_4 flux ±prediction variance sd (pink shading). The blue line on regression plots is a 1:1 line.

4. Discussion

4.1. Comparisons With Previous Wetland CH_4 Studies

Limited studies incorporate long-term information on ecosystem-scale CH_4 dynamics in salt marshes. Furthermore, most studies have based their analyses on more traditional methods, reporting that temperature, PAR, plant productivity, or some proxy (e.g., GPP, biomass, chlorophyll concentration), water level, and salinity are important predictors for CH_4 fluxes (Abdul-Aziz et al., 2018; Huertas et al., 2019; Martin & Moseman-Valtierra, 2017; Poffenbarger et al., 2011). Despite differing temporal averaging periods (e.g., daytime, nighttime, year-round, multi-year) and different model structures (e.g., linear regression, multivariate canonical correlation, multivariate generalized least squares), multiple approaches have also been able to identify the importance of temperature, DO, and Patm for CH_4 dynamics (Hill & Vargas, 2022; Vázquez-Lule & Vargas, 2021). Other multi-site studies have also identified comparable predictor variables with linear and nonlinear methods, especially temperature components, in non-tidal freshwater wetlands (e.g., Knox et al., 2021). However, there is increasing evidence that the effect of these variables and others, such as water level and GPP, are more complex and influence CH_4 fluxes in freshwater wetlands across various temporal scales (Sturtevant et al., 2016).

Our results using CCM indicate that the effects of GPP are highly dependent on the time domain at multiple scales (seasonal and diurnal) and multivariate interactions among variables. While linear models have identified that similar variables influence CH_4 fluxes, those methods have limitations in identifying dependencies, lags, and complex interrelationships. These limitations are overcome when applying CCM and we demonstrate interrelationships among variables and the relevance of lags that influence CH_4 dynamics (Figures 2–5).

Several studies based on non-tidal freshwater wetlands have successfully applied alternative nonlinear analysis methods (Knox et al., 2021; Sturtevant et al., 2016) or machine learning approaches such as ANN's or random forest techniques (Abbasi et al., 2019; Morin et al., 2017; Rey-Sanchez et al., 2018; Zaki & Abdul-Aziz, 2022; Zhu et al., 2013). In these non-tidal freshwater wetlands, interactions regulating fluxes do not include the same dynamics found within tidal wetlands, including frequent oscillation of water level and subsequent modulation of sediment salinity, dissolved oxygen, and redox conditions (Capooci & Vargas, 2022; Vázquez-Lule & Vargas, 2021). Further, dominant vegetation species differ, which can influence the biogeochemical conditions of the sediments and CH_4 production (Gao et al., 2018; Seyfferth et al., 2020; Yuan et al., 2016). Despite differences, these studies also show that both linear and nonlinear approaches identify the strongest relevant drivers, yet incomplete results from solely applying linear methods limit the full mechanistic understanding of the system (Sturtevant et al., 2016). Specifically, issues of cross-correlation can restrict which variables are included to satisfy model requirements, and important lags and interrelationships fail to be identified. In fact, tidal saltwater wetlands have been purposely excluded from several FLUXNET- CH_4 analyses because they do not follow the general pattern of linear relationships defined by freshwater wetlands, and an overall lack of data from these highly dynamic ecosystems creates difficulties when attempting to generalize across multiple sites (Chang et al., 2021; Delwiche et al., 2021; Knox et al., 2021).

In limited cases where nonlinear methods are applied, findings largely support our results, demonstrating lags with GPP, temperature, and water level, but with temporal synchrony with VPD and energy fluxes (Delwiche et al., 2021). For example, in a multi-site synthesis study of freshwater sites, median seasonal lags associated with water level extended 17 ± 11 days, 8 ± 16, and 5 ± 14 days for Tair and Tsoil, respectively, and were synchronous for Patm while at the diel scale, GPP was lagged up to 4 hr and energy fluxes and VPD were synchronous (<1 hr) (Knox et al., 2021). A similar study from a forested/shrub wetland found CH_4 lags associated with GPP extending up to 60 days (Turner et al., 2021), potentially indicating different time dependencies based on vegetation type and structure. There is overwhelming evidence supporting that temporal lags exist between multiple environmental variables and CH_4 fluxes across different types of wetlands. Thus, it is important to explore the applicability of methods such as CCM to improve our understanding of the biophysical drivers of CH_4 fluxes at different time scales and with different time lags.

4.2. Seasonal CH_4 Dynamics

Our results indicate CH_4 seasonal dynamics were most associated with temperature components, GPP, and DO. Previous studies showed that predictors such as Level, Patm, and VPD are important in a linear multivariate context but have lower importance when data is analyzed with CCM (Hill & Vargas, 2022; Vázquez-Lule & Vargas, 2021). Differences may arise due to the longer time series used in this study; therefore, several conditions may have changed. We propose that Level, Patm, and VPD are less strongly coupled with CH_4 activity at this scale due to: (a) limited occurrence as with transient low-pressure systems, which promote CH_4 emissions and rarely exert influence on scales extending beyond several days (Figure 2b) (Knox et al., 2021; Mønster et al., 2019; Tokida et al., 2007); or (b) indirect mechanisms as with Patm and pressurized gas flow (Björn et al., 2022; Zhang & Ding, 2011), and VPD limiting stomatal conductance and the possible decrease in plant-mediated transport. At the seasonal scale, temperature is a strong predictor in temperate ecosystems because it regulates the window of active plant growth and belowground microbial metabolic rates (Yvon-Durocher et al., 2014; Zhu et al., 2019), influencing below-ground storage pools and, ultimately, sediment-atmosphere fluxes (Capooci & Vargas, 2022; Reid et al., 2013). GPP also has strong coupling and may suggest there is connectivity or flow between plant photoassimilates and methanogens in the rhizosphere, which increases with seasonal biomass development. We observed a 32-day median lag time between GPP and effects on CH_4 flux, similar to the lag identified for temperature (35 days), which may indicate structural changes in the vegetation, such as the development of aerenchyma tissues, are responsible for the observed seasonal increase in CH_4 flux (Granse et al., 2022). Weaker couplings were associated with physical variables such as Patm, and lag times for these variables were much shorter. Thus, these differential groupings based on coupling strength may provide insights into how biological versus physical processes operate at different temporal scales.

Salinity, when used as a proxy of sulfate availability, has previously been identified as an important daily-scale predictor by linear modeling but had no direct causal influence on seasonal CH_4 fluxes in this study. While salinity causes direct inhibitory effects for acetoclastic and hydrogenotrophic methanogenesis by limiting the availability of substrates via microbial competition in most wetlands (Reddy et al., 2022), there is evidence for the presence of methylotrophic bacteria in salt marshes which produce CH_4 from non-competitive substrates resulting in elevated emissions despite the presence of sulfate (Capooci & Vargas, 2022; Capooci et al., 2024; Seyfferth et al., 2020). Evidence to support this phenomenon exists from a variety of wetland studies that contain *S. alterniflora* and emit methane above or at the high-end of a widely accepted CH_4-sulfate threshold (Comer-Warner et al., 2022; Huertas et al., 2019; Oremland et al., 1982; Poffenbarger et al., 2011). We propose that the elevated emissions, especially during senescence, are tied to the release of secondary plant compounds (osmolytes) associated with *S. alterniflora* (which we did not measure) including glycine betaine and dimethyl sulfoniopropionate which are broken down via fermentation to trimethylamine and dimethyl sulfide and are exclusively utilized by methylotrophic methanogens (Husband & Kiene, 2007; Jones et al., 2019). It is also important to note that this marsh rarely experiences salinity extremes over 20ppt, thus sites influenced by higher salinity may experience different characteristics.

4.3. Diurnal CH_4 Dynamics

Our results indicate that diurnal CH_4 dynamics during the growing phenoperiod are tied by multiple factors with many potential interdependencies among variables, yet variables with the highest association were Level, Patm, Sal, DO, and Tsoil. This may indicate that CH_4 fluxes over the diurnal course are influenced by both biochemical

factors likely tied to plant and microbial activity (Sal, DO, Tsoil) and physical factors likely tied to emissions (Level, Patm) (Knox et al., 2021; Liu et al., 2019; Moore & Roulet, 1993; Reid et al., 2015). While several studies have made attempts at reducing this level of complexity by applying parsimonious models that only incorporate the most important drivers (via linear methods) (Abdul-Aziz et al., 2018; Baird et al., 2019; Levy et al., 2012), this may only be useful for generating coarse-scale information. Other studies have applied more complex process-based models, although these require an extensive mechanistic understanding and often experience difficulties when moving across study sites (Li et al., 2016; Zhang et al., 2020), where interacting variables and driving processes can differ considerably (Krauss et al., 2016; Rosentreter et al., 2021). This can limit the range of potential applications and may be less relevant for coastal wetlands where relationships can differ greatly from site to site.

Our results indicate that the dormancy phenoperiod is comparatively simple. Variables with the highest association were Level, DO, and Sal. This is also supported by considerably less interconnection between variables. Considering the lack of active vegetation, we can assume mechanisms related to these predictors change in relation to the growing or year-round daily averaging periods (Bansal et al., 2020; Reid et al., 2013). Although the relationship is weak, coupling between CH_4 and Sal increases following the end of senescence and the preceding seasonal peak in emissions. Because vegetation is no longer present, the flow of photoassimilates stops, and the availability of osmolyte byproducts likely decreases within sediments. Thus, Sal may become more relevant during dormancy as competition between sulfate-reducing bacteria and methanogens likely increases (Derby et al., 2021; Poffenbarger et al., 2011), while the spatial separation between production zones at depth may be less exposed to sulfate fluctuations from tidal exchange (Koebsch et al., 2019). Further, plant-mediated transport is curtailed, likely leading to greater importance of conditions at the sediment interface (Wang & Han, 2005). This is supported by the lack of association between variables such as GPP, LE, and H_2O flux. This could also explain the importance of DO in tidal waters, which reaches a concentration peak during dormancy, likely influencing CH_4 oxidation rates. In either case, the top hourly predictor identified for both growing and dormancy phenoperiods is Level, which oscillates between low and high tides at six-hour intervals but also shifts on a 14-day spring/neap tide and is highly tied to fluctuations of DO and Sal (Vázquez-Lule & Vargas, 2021). Our results indicate that while all these variables are related and often highly cross-correlated with linear methods, each of these variables likely exerts a unique influence on CH_4 dynamics, yet there is also strong interdependence with how these variable relationships change in time, highlighting the importance of incorporating true nonlinear analysis methods.

4.4. Relevance of Time Lags

On a seasonal/multiday scale, almost all variables identified by CCM were associated with lag times where potential influence is exerted across several consecutive days or weeks. Variables with higher identified associations (temperature components and GPP) had medium lag times (i.e., "slow") near 3–5 weeks, likely associated with the possible threshold effect with the temperature-driven initiation of plant growth (O'Connell et al., 2020), or increased production and transport of photoassimilates to the rhizosphere (Knox et al., 2021). This lag time (3 weeks) was also associated with the effect of salinity on GPP, likely indicating increases in plant osmolyte production coinciding with initial spring biomass accumulation (Husband & Kiene, 2007; Mulholland & Otte, 2000). It is important to recognize that we are measuring CH_4 fluxes (the physical process of release); thus, these observed lags are also likely associated with the disconnection between production and observed fluxes. The shortest lags exert immediate (<1 week) (i.e., "fast") but also prolonged impact extending up to 1 week for Level, Patm, and RH and up to 4 weeks for DO. This effect from Level is likely a result of high/low water levels tied to spring/neap tide cycles, which oscillate on a 6–7-day period. Yet, there are also fluctuations at shorter time periods, both of which impact soil water content and biogeochemical conditions of the sediments (Seyfferth et al., 2020). Tidal waters also directly influence salinity and DO levels within sediments, but the effect of DO is prolonged and likely tied to its strong influence on GPP, as shown by our results (Figure 4). The effects of Patm and RH are likely tied to mesoscale circulation and air mass transit which modify the air column and provide a physical forcing mechanism (Tokida et al., 2007). The longest lag times were associated with LE, H_2O flux, and PAR, which likely represents a major seasonal oscillation driven by solar angle and changes in available radiation (Guo et al., 2010). While only identified as having weak associations, there were no lags associated with WSpd or Precip, indicating an effect exclusively at the sub-daily level as, in most cases, the occurrence of wind or rain rarely extends into multi-day events.

During the growing phenoperiod, variables identified by CCM (Level, Patm, Sal, DO, Tsoil) all operated at different peak lag times, highlighting the complexity of observing and measuring fluxes during this time. The highest-ranking variable identified, (Level) exerts influence over the entire 24-hr period yet peaks at 0–5 hr and 20–24 hr, near when Sal was influential, which is likely tied to semi-diurnal tidal cycling and water levels which are typically higher during nighttime high tide (Forbrich & Giblin, 2015). Influence over the entire 24-hr period may be due to a smearing-out effect as the tide shifts its range an hour each day. Patm and DO (moderately causal) were associated with a zero-lag time but the effect of Patm extended up to 5 hr. These lags are likely related to fast (immediate) oxidation activity across sediment, daily pressure fluctuations, and convective flow-through transport of CH_4 via plant-mediated transport driven by solar activity (Ding & Cai, 2007; Kim et al., 1999). Although the overall causality was weaker and distributed across variables, many of the fast variables during the growing phenoperiod are related to energy exchange dynamics (LE and H) and tied to changes in evapotranspiration (H_2O flux, VPD, RH). This is likely explained by combined evaporation from saturated sediments where CH_4 has accumulated in porewater, evaporation from areas of open water that receive a lateral influx of dissolved CH_4, and plant-mediated transport factors reliant on stomatal activity, which channel dissolved CH_4 in the transpiration stream (Megonigal & Guenther, 2008; Trifunovic et al., 2020). We found GPP is both a fast and slow variable which could indicate a supply of photoassimilates is triggered upon initiation of morning photosynthesis but with lags extending up to 8 hr when photosynthesis gears down in the evening.

During the dormancy phenoperiod, variables identified by CCM (Level, Sal, DO) were found to have immediate influence but were influential at lag times extending up to 5–10 hr, highlighting the importance of tidal activity and modulation of associated variables (Sal and DO). While the remaining variables comprised weaker associations, several interesting patterns emerged. In contrast to the slower effect of Tair during the growing phenoperiod, Tair was a fast variable with short lag times in dormancy, while the effect of Tsoil had longer lags, up to 9 hr, potentially indicating a connection to microbial activity and temperature thresholds associated with CH_4 production (Chadburn et al., 2020). All highly associated variables were related to tidal activity (Level, DO, Sal), indicating that hydrological factors and the riverine-ocean connectivity become crucial during the dormancy phenoperiod. The shorter lag times found during this phenoperiod may also indicate more direct coupling with physical factors and less complex interactions involving the presence of vegetation, such as substrate supply and plant-mediated transport (Vázquez-Lule & Vargas, 2021). Taken together, these results highlight the multi-mechanistic activities and processes that regulate CH_4 fluxes.

4.5. Multivariate EDM Modeling

This study demonstrates high complexity in the biophysical controls of CH_4 fluxes in tidal wetlands. These results are based on high-frequency measurements and long-term observations (5 years) contributing to our understanding of CH_4 dynamics. This model captured most of the higher magnitude fluctuations and high emission peaks during the growing phenoperiod yet omitted higher magnitude fluctuations during senescence. Despite good performance, this model still considerably underpredicted during senescence and overpredicted during green-up. Consequently, these transitions represent a challenge as rapid metabolic and structural changes happen in the plant canopy while microbial community activity could also be altered (Capooci et al., 2024; Vazquez-Lule et al., 2022). Although we included the full suite of associated variables identified by CCM, this could indicate that additional variables omitted or not measured (e.g., sediment redox potential, biomass, sediment substrate availability) are essential to explain these unusually high fluxes during senescence. While we scaled predictor variables, adding variables may still cause distortion in the state space, ultimately leading to a larger uncertainty. Thus, simpler models focusing on key predictor variables could be preferable to saturated models with complex interpretability.

5. Conclusion

We demonstrate that nonlinear state space methods can be used to uncover complex dynamics and interdependencies among possible predictors and their influence on CH_4 flux. The technique can tease apart not only the strength of causal variables but also identify lags and complex variable interconnections. Overall, CCM was able to identify and rank multiple variables while providing a holistic picture of variable interactions and lagged relationships, which is critical for an accurate mechanistic understanding of system behavior. We found that seasonal CH_4 emissions were highly influenced by changes in temperature of soil, water, and air, DO, and GPP with lag times ranging from 0 to 35 days. Diurnal growing season emissions were highly influenced by

Level, Patm, Sal, DO, and Tsoil with lag times ranging from 0 to 23 hr while diurnal dormancy season emissions were influenced by Level, Sal, and DO with shorter lag times (0–10 hr). We highlight that CCM is a powerful technique that provides mechanistic information regarding potential driver associations, lags, and interconnectivity among an extensive collection of potentially important variables. Therefore, by complementing CCM with multivariate EDM we can generate interpretable empirical models that provide insights into controlling mechanisms of ecosystem processes.

While we included many ancillary variables typically measured at wetland FLUXNET sites to parameterize our EDM model, results could change if a different set of variables were included, as with any empirical modeling approach. Thus, we encourage the scientific community to test the applicability of CCM/EDM across different wetland sites. Future work should also focus on expanding this analysis to define lag windows for the network maps, and better examination of how this novel technique compares to other nonlinear methods.

Data Availability Statement

Meteorological (station: delsjmet-p) and water quality (station: Aspen Landing) data are available from the National Estuarine Research Reserve's Centralized Data Management Office (CDMO; NOAA NERRS, 2023). Phenological data are available from the PhenoCam network (site: stjones; Seyednasrollah et al., 2019). Eddy covariance data are available via AmeriFlux (US-StJ; Vargas, 2020).

Acknowledgments
This research was supported by the National Science Foundation (#1652594) and the US Department of Energy (#DE-SC0023099 and #DE-SC0022185). We thank the onsite support from the Delaware National Estuarine Research Reserve (DNERR) and helpful guidance on the EDM method from Joseph Park. The authors acknowledge the land on which they conducted this study is the traditional home of the Lenni-Lenape tribal nation (Delaware nation).

References

Abbasi, T., Abbasi, T., Luithui, C., & Abbasi, S. A. (2019). Modelling methane and nitrous oxide emissions from rice paddy wetlands in India using artificial neural networks (ANNs). *Water*, *11*(10), 2169. https://doi.org/10.3390/w11102169

Abdul-Aziz, O. I., Ishtiaq, K. S., Tang, J. W., Moseman-Valtierra, S., Kroeger, K. D., Gonneea, M. E., et al. (2018). Environmental controls, emergent scaling, and predictions of greenhouse gas (GHG) Fluxes in coastal salt marshes. *Journal of Geophysical Research: Biogeosciences*, *123*(7), 2234–2256. https://doi.org/10.1029/2018jg004556

Al-Haj, A. N., & Fulweiler, R. W. (2020). A synthesis of methane emissions from shallow vegetated coastal ecosystems. *Global Change Biology*, *26*(5), 2988–3005. https://doi.org/10.1111/gcb.15046

Baird, A., Green, S., Brown, E., & Dooling, G. (2019). Modelling time-integrated fluxes of CO_2 and CH_4 in peatlands: A review. *Mires & Peat*, *24*.

Baldocchi, D. D. (2003). Assessing the eddy covariance technique for evaluating carbon dioxide exchange rates of ecosystems: Past, present and future. *Global Change Biology*, *9*(4), 479–492. https://doi.org/10.1046/j.1365-2486.2003.00629.x

Bansal, S., Johnson, O. F., Meier, J., & Zhu, X. (2020). Vegetation affects timing and location of wetland methane emissions. *Journal of Geophysical Research: Biogeosciences*, *125*(9), e2020JG005777. https://doi.org/10.1029/2020jg005777

Bartlett, K. B., Bartlett, D. S., Harriss, R. C., & Sebacher, D. I. (1987). Methane emissions along a salt marsh salinity gradient. *Biogeochemistry*, *4*(3), 183–202. https://doi.org/10.1007/bf02187365

Björn, L. O., Middleton, B. A., Germ, M., & Gaberščik, A. (2022). Ventilation systems in wetland plant species. *Diversity*, *14*(7), 517. https://doi.org/10.3390/d14070517

Borges, A. V., & Abril, G. (2011). In E. Wolanski & D. McLusky (Eds.), *Carbon dioxide and methane dynamics in estuaries. Vol 5: Biogeochemistry*.

Bridgham, S. D., Cadillo-Quiroz, H., Keller, J. K., & Zhuang, Q. L. (2013). Methane emissions from wetlands: Biogeochemical, microbial, and modeling perspectives from local to global scales. *Global Change Biology*, *19*(5), 1325–1346. https://doi.org/10.1111/gcb.12131

Capooci, M., Barba, J., Seyfferth, A. L., & Vargas, R. (2019). Experimental influence of storm-surge salinity on soil greenhouse gas emissions from a tidal salt marsh. *The Science of the Total Environment*, *686*, 1164–1172. https://doi.org/10.1016/j.scitotenv.2019.06.032

Capooci, M., Seyfferth, A. L., Tobias, C., Wozniak, A. S., Hedgpeth, A., Bowen, M., et al. (2024). High methane concentrations in tidal salt marsh soils: Where does the methane go? *Global Change Biology*, *30*(1), e17050. https://doi.org/10.1111/gcb.17050

Capooci, M., & Vargas, R. (2022). Trace gas fluxes from tidal salt marsh soils: Implications for carbon-sulfur biogeochemistry. *Biogeosciences*, *19*, 4655–4670. https://doi.org/10.5194/bg-19-4655-2022

Chadburn, S. E., Aalto, T., Aurela, M., Baldocchi, D., Biasi, C., Boike, J., et al. (2020). Modeled microbial dynamics explain the apparent temperature sensitivity of wetland methane emissions. *Global Biogeochemical Cycles*, *34*(11), e2020GB006678. https://doi.org/10.1029/2020gb006678

Chang, C.-W., Ushio, M., & Hsieh, C.-H. (2017). Empirical dynamic modeling for beginners. *Ecological Research*, *32*(6), 785–796. https://doi.org/10.1007/s11284-017-1469-9

Chang, K.-Y., Riley, W. J., Knox, S. H., Jackson, R. B., McNicol, G., Poulter, B., et al. (2021). Substantial hysteresis in emergent temperature sensitivity of global wetland CH_4 emissions. *Nature Communications*, *12*, 1–10. https://doi.org/10.1038/s41467-021-22452-1

Comer-Warner, S. A., Ullah, S., Reyes, W. A., Krause, S., & Chmura, G. L. (2022). *Spartina alterniflora* has the highest methane emissions in a St. Lawrence estuary salt marsh. *Environmental Research-Ecology*, *1*, 011003. https://doi.org/10.1088/2752-664x/ac706a

Conrad, R. (2020). Importance of hydrogenotrophic, aceticlastic and methylotrophic methanogenesis for methane production in terrestrial, aquatic and other anoxic environments: A mini review. *Pedosphere*, *30*(1), 25–39. https://doi.org/10.1016/s1002-0160(18)60052-9

Dean, J. F., Middelburg, J. J., Röckmann, T., Aerts, R., Blauw, L. G., Egger, M., et al. (2018). Methane feedbacks to the global climate system in a warmer world. *Reviews of Geophysics*, *56*(1), 207–250. https://doi.org/10.1002/2017rg000559

Delwiche, K. B., Knox, S. H., Malhotra, A., Fluet-Chouinard, E., McNicol, G., Feron, S., et al. (2021). FLUXNET-CH4: A global, multi-ecosystem dataset and analysis of methane seasonality from freshwater wetlands. *Earth System Science Data*, *13*(7), 3607–3689. https://doi.org/10.5194/essd-13-3607-2021

Derby, R. K., Needelman, B. A., Roden, A. A., & Megonigal, J. P. (2021). Stratifying by vegetation and hydrology improves tidal marsh methane emission accounting. *Environmental Sciences*.

Deyle, E. R., May, R. M., Munch, S. B., & Sugihara, G. (2016). Tracking and forecasting ecosystem interactions in real time. *Proceedings: Biological Science*, *283*, 20152258. https://doi.org/10.1098/rspb.2015.2258

Dietze, M. C., Vargas, R., Richardson, A. D., Stoy, P. C., Barr, A. G., Anderson, R. S., et al. (2011). Characterizing the performance of ecosystem models across time scales: A spectral analysis of the North American carbon program site-level synthesis. *Journal of Geophysical Research: Biogeosciences*, *116*(G4), G04029. https://doi.org/10.1029/2011jg001661

Ding, W. X., & Cai, Z. C. (2007). Methane emission from natural wetlands in China: Summary of years 1995-2004 studies. *Pedosphere*, *17*(4), 475–486. https://doi.org/10.1016/s1002-0160(07)60057-5

Fan, H., Meng, Y., Wang, D., Zhao, Y., & Zhao, C. (2020). Detecting time-delayed causations in coal mill based on convergent cross mapping. In *2020 35th youth academic annual conference of Chinese association of automation (YAC)* (pp. 347–352). IEEE.

Filippa, G., Cremonese, E., Migliavacca, M., Galvagno, M., Forkel, M., Wingate, L., et al. (2016). Phenopix: A R package for image-based vegetation phenology. *Agricultural and Forest Meteorology*, *220*, 141–150. https://doi.org/10.1016/j.agrformet.2016.01.006

Forbrich, I., & Giblin, A. E. (2015). Marsh-atmosphere CO_2 exchange in a New England salt marsh. *Journal of Geophysical Research: Biogeosciences*, *120*(9), 1825–1838. https://doi.org/10.1002/2015jg003044

Gao, G. F., Li, P. F., Shen, Z. J., Qin, Y. Y., Zhang, X. M., Ghoto, K., et al. (2018). Exotic *Spartina alterniflora* invasion increases CH_4 while reduces CO_2 emissions from mangrove wetland soils in southeastern China. *Scientific Reports*, *8*(1), 9243. https://doi.org/10.1038/s41598-018-27625-5

Granse, D., Titschack, J., Ainouche, M., Jensen, K., & Koop-Jakobsen, K. (2022). Subsurface aeration of tidal wetland soils: Root-system structure and aerenchyma connectivity in Spartina (Poaceae). *Science of the Total Environment*, *802*, 149771. https://doi.org/10.1016/j.scitotenv.2021.149771

Gu, L., Post, W. M., Baldocchi, D. D., Black, T. A., Suyker, A. E., Verma, S. B., et al. (2009). Characterizing the seasonal dynamics of plant community photosynthesis across a range of vegetation types. In *Phenology of ecosystem processes* (pp. 35–58). Springer.

Guo, H. Q., Zhao, B., Chen, J. Q., Yan, Y. E., Li, B., & Chen, J. K. (2010). Seasonal changes of energy fluxes in an estuarine wetland of Shanghai, China. *Chinese Geographical Science*, *20*(1), 23–29. https://doi.org/10.1007/s11769-010-0023-2

Hill, A. C., & Vargas, R. (2022). Methane and carbon dioxide fluxes in a temperate tidal salt Marsh: Comparisons between plot and ecosystem measurements. *Journal of Geophysical Research: Biogeosciences*, *127*(7), e2022JG006943. https://doi.org/10.1029/2022jg006943

Hill, A. C., Vázquez-Lule, A., & Vargas, R. (2021). Linking vegetation spectral reflectance with ecosystem carbon phenology in a temperate salt marsh. *Agricultural and Forest Meteorology*, *307*, 108481. https://doi.org/10.1016/j.agrformet.2021.108481

Hsieh, C.-H., Glaser, S. M., Lucas, A. J., & Sugihara, G. (2005). Distinguishing random environmental fluctuations from ecological catastrophes for the North Pacific Ocean. *Nature*, *435*(7040), 336–340. https://doi.org/10.1038/nature03553

Huertas, I. E., de la Paz, M., Perez, F. F., Navarro, G., & Flecha, S. (2019). Methane emissions from the salt marshes of Donana wetlands: Spatio-temporal variability and controlling factors. *Frontiers in Ecology and Evolution*, *7*. https://doi.org/10.3389/fevo.2019.00032

Husband, J. D., & Kiene, R. P. (2007). Occurrence of dimethylsulfoxide in leaves, stems, and roots of *Spartina alterniflora*. *Wetlands*, *27*(2), 224–229. https://doi.org/10.1672/0277-5212(2007)27[224:oodils]2.0.co;2

Jackson, R. B., Saunois, M., Bousquet, P., Canadell, J. G., Poulter, B., Stavert, A. R., et al. (2020). Increasing anthropogenic methane emissions arise equally from agricultural and fossil fuel sources. *Environmental Research Letters*, *15*(7), 071002. https://doi.org/10.1088/1748-9326/ab9ed2

Jones, H. J., Kröber, E., Stephenson, J., Mausz, M. A., Jameson, E., Millard, A., et al. (2019). A new family of uncultivated bacteria involved in methanogenesis from the ubiquitous osmolyte glycine betaine in coastal saltmarsh sediments. *Microbiome*, *7*(1), 120. https://doi.org/10.1186/s40168-019-0732-4

Kennish, M. J. (2019). The national estuarine research reserve system: A review of research and monitoring initiatives. *Open Journal of Ecology*, *9*(03), 50–65. https://doi.org/10.4236/oje.2019.93006

Kim, D. S. (2007). Greenhouse Gas (CH_4, CO_2, N_2O) emissions from estuarine tidal and wetland and their characteristics. *Journal of Korean Society for Atmospheric Environment*, *23*(2), 225–241. https://doi.org/10.5572/kosae.2007.23.2.225

Kim, J., Verma, S. B., & Billesbach, D. P. (1999). Seasonal variation in methane emission from a temperate Phragmites-dominated marsh: Effect of growth stage and plant-mediated transport. *Global Change Biology*, *5*(4), 433–440. https://doi.org/10.1046/j.1365-2486.1999.00237.x

Kim, Y., Johnson, M. S., Knox, S. H., Black, T. A., Dalmagro, H. J., Kang, M., et al. (2020). Gap-filling approaches for eddy covariance methane fluxes: A comparison of three machine learning algorithms and a traditional method with principal component analysis. *Global Change Biology*, *26*(3), 1499–1518. https://doi.org/10.1111/gcb.14845

Knox, S. H., Bansal, S., McNicol, G., Schafer, K., Sturtevant, C., Ueyama, M., et al. (2021). Identifying dominant environmental predictors of freshwater wetland methane fluxes across diurnal to seasonal time scales. *Global Change Biology*, *27*(15), 3582–3604. https://doi.org/10.1111/gcb.15661

Koebsch, F., Winkel, M., Liebner, S., Liu, B., Westphal, J., Schmiedinger, I., et al. (2019). Sulfate deprivation triggers high methane production in a disturbed and rewetted coastal peatland. *Biogeosciences*, *16*(9), 1937–1953. https://doi.org/10.5194/bg-16-1937-2019

Krauss, K. W., Holm, G. O., Perez, B. C., McWhorter, D. E., Cormier, N., Moss, R. F., et al. (2016). Component greenhouse gas fluxes and radiative balance from two deltaic marshes in Louisiana: Pairing chamber techniques and eddy covariance. *Journal of Geophysical Research: Biogeosciences*, *121*(6), 1503–1521. https://doi.org/10.1002/2015jg003224

Kuhn, M. (2008). Building predictive models in R using the caret package. *Journal of Statistical Software*, *28*(5), 1–26. https://doi.org/10.18637/jss.v028.i05

Levy, P. E., Burden, A., Cooper, M. D., Dinsmore, K. J., Drewer, J., Evans, C., et al. (2012). Methane emissions from soils: Synthesis and analysis of a large UK data set. *Global Change Biology*, *18*(5), 1657–1669. https://doi.org/10.1111/j.1365-2486.2011.02616.x

Li, C. (2007). Quantifying greenhouse gas emissions from soils: Scientific basis and modeling approach. *Soil Science & Plant Nutrition*, *53*(4), 344–352. https://doi.org/10.1111/j.1747-0765.2007.00133.x

Li, T. T., Xie, B. H., Wang, G. C., Zhang, W., Zhang, Q., Vesala, T., & Raivonen, M. (2016). Field-scale simulation of methane emissions from coastal wetlands in China using an improved version of CH4MOD(wetland). *Science of the Total Environment*, *559*, 256–267. https://doi.org/10.1016/j.scitotenv.2016.03.186

Li, Y., Wang, D., Chen, Z., Chen, J., Hu, H., & Wang, R. (2021). Methane emissions during the tide cycle of a Yangtze Estuary salt marsh. *Atmosphere*, *12*(2), 245. https://doi.org/10.3390/atmos12020245

Liu, L. J., Wang, D. Q., Chen, S., Yu, Z. J., Xu, Y. K., Li, Y., et al. (2019). Methane emissions from estuarine coastal wetlands: Implications for global change effect. *Soil Science Society of America Journal*, *83*(5), 1368–1377. https://doi.org/10.2136/sssaj2018.12.0472

Lu, X., Zhou, Y., Zhuang, Q., Prigent, C., Liu, Y., & Teuling, A. (2018). Increasing methane emissions from natural land ecosystems due to sea-level rise. *Journal of Geophysical Research: Biogeosciences*, *123*(5), 1756–1768. https://doi.org/10.1029/2017jg004273

Martin, R. M., & Moseman-Valtierra, S. (2017). Different short-term responses of greenhouse gas fluxes from salt marsh mesocosms to simulated global change drivers. *Hydrobiologia*, *802*(1), 71–83. https://doi.org/10.1007/s10750-017-3240-1

McKenna, T., Callahan, J., Medlock, C., & Bates, N. (2018). Creation of improved accuracy LiDAR-based digital elevation models for the St. Jones River and blackbird creek watersheds. Newark: Delaware geologic survey, technical report (pp. 1–30).

Megonigal, J. P., & Guenther, A. B. (2008). Methane emissions from upland forest soils and vegetation. *Tree Physiology*, *28*(4), 491–498. https://doi.org/10.1093/treephys/28.4.491

Mønster, J., Kjeldsen, P., & Scheutz, C. (2019). Methodologies for measuring fugitive methane emissions from landfills – A review. *Waste Management*, *87*, 835–859. https://doi.org/10.1016/j.wasman.2018.12.047

Moore, T. R., & Roulet, N. T. (1993). Methane flux: Water table relations in northern wetlands. *Geophysical Research Letters*, *20*(7), 587–590. https://doi.org/10.1029/93gl00208

Morin, T. H. (2019). Advances in the eddy covariance approach to CH_4 monitoring over two and a half decades. *Journal of Geophysical Research-Biogeosciences*, *124*(3), 453–460. https://doi.org/10.1029/2018jg004796

Morin, T. H., Bohrer, G., Stefanik, K. C., Rey-Sanchez, A. C., Matheny, A. M., & Mitsch, W. J. (2017). Combining eddy-covariance and chamber measurements to determine the methane budget from a small, heterogeneous urban floodplain wetland park. *Agricultural and Forest Meteorology*, *237*, 160–170. https://doi.org/10.1016/j.agrformet.2017.01.022

Mulholland, M. M., & Otte, M. L. (2000). Effects of varying sulphate and nitrogen supply on DMSP and glycine betaine levels in *Spartina anglica*. *Journal of Sea Research*, *43*(3–4), 199–207. https://doi.org/10.1016/s1385-1101(00)00015-0

Munch, S. B., Giron-Nava, A., & Sugihara, G. (2018). Nonlinear dynamics and noise in fisheries recruitment: A global meta-analysis. *Fish and Fisheries*, *19*(6), 964–973. https://doi.org/10.1111/faf.12304

Munch, S. B., Rogers, T. L., & Sugihara, G. (2023). Recent developments in empirical dynamic modelling. *Methods in Ecology and Evolution/British Ecological Society*, *14*(3), 732–745. https://doi.org/10.1111/2041-210x.13983

Murray, F. W. (1967). On the computation of saturation vapor pressure. *Journal of Applied Meteorology and Climatology*, *6*(1), 203–204. https://doi.org/10.1175/1520-0450(1967)006<0203:otcosv>2.0.co;2

Neubauer, S. C., & Megonigal, J. P. (2019). Moving beyond global warming potentials to quantify the climatic role of ecosystems. *Ecosystems*, *22*, 1931–1932.

NOAA National Estuarine Research Reserve System (NERRS). (2023). System-wide monitoring program [Dataset]. Data accessed from the NOAA NERRS Centralized Data Management Office. Retrieved from http://www.nerrsdata.org

O'Connell, J. L., Alber, M., & Pennings, S. C. (2020). Microspatial differences in soil temperature cause phenology change on par with long-term climate warming in salt marshes. *Ecosystems*, *23*(3), 498–510. https://doi.org/10.1007/s10021-019-00418-1

Oremland, R. S., Marsh, L. M., & Polcin, S. (1982). Methane production and simultaneous sulphate reduction in anoxic, salt marsh sediments. *Nature*, *296*(5853), 143–145. https://doi.org/10.1038/296143a0

Oremland, R. S., & Polcin, S. (1982). Methanogenesis and sulfate reduction: Competitive and noncompetitive substrates in estuarine sediments. *Applied and Environmental Microbiology*, *44*(6), 1270–1276. https://doi.org/10.1128/aem.44.6.1270-1276.1982

Park, J., & Stabenau, E. (2022). Dynamics of total phosphate in the greater Everglades. *Ecological Indicators*, *145*, 109574. https://doi.org/10.1016/j.ecolind.2022.109574

Poffenbarger, H. J., Needelman, B. A., & Megonigal, J. P. (2011). Salinity influence on methane emissions from tidal marshes. *Wetlands*, *31*(5), 831–842. https://doi.org/10.1007/s13157-011-0197-0

Reddy, K. R., DeLaune, R. D., & Inglett, P. W. (2022). *Biogeochemistry of wetlands: Science and applications*. CRC press. https://doi.org/10.1201/9780429155833

Reichstein, M., Falge, E., Baldocchi, D., Papale, D., Aubinet, M., Berbigier, P., et al. (2005). On the separation of net ecosystem exchange into assimilation and ecosystem respiration: Review and improved algorithm. *Global Change Biology*, *11*(9), 1424–1439. https://doi.org/10.1111/j.1365-2486.2005.001002.x

Reid, M. C., Pal, D. S., & Jaffe, P. R. (2015). Dissolved gas dynamics in wetland soils: Root-mediated gas transfer kinetics determined via push-pull tracer tests. *Water Resources Research*, *51*(9), 7343–7357. https://doi.org/10.1002/2014wr016803

Reid, M. C., Tripathee, R., Schafer, K. V. R., & Jaffe, P. R. (2013). Tidal marsh methane dynamics: Difference in seasonal lags in emissions driven by storage in vegetated versus unvegetated sediments. *Journal of Geophysical Research-Biogeosciences*, *118*(4), 1802–1813. https://doi.org/10.1002/2013jg002438

Rey-Sanchez, A. C., Morin, T. H., Stefanik, K. C., Wrighton, K., & Bohrer, G. (2018). Determining total emissions and environmental drivers of methane flux in a Lake Erie estuarine marsh. *Ecological Engineering*, *114*, 7–15. https://doi.org/10.1016/j.ecoleng.2017.06.042

Rosentreter, J. A., Al-Haj, A. N., Fulweiler, R. W., & Williamson, P. (2021). Methane and nitrous oxide emissions complicate coastal blue carbon assessments. *Global Biogeochemical Cycles*, *35*(2), e2020GB006858. https://doi.org/10.1029/2020gb006858

Schafer, K. V. R., Tripathee, R., Artigas, F., Morin, T. H., & Bohrer, G. (2014). Carbon dioxide fluxes of an urban tidal marsh in the Hudson-Raritan estuary. *Journal of Geophysical Research-Biogeosciences*, *119*(11), 2065–2081. https://doi.org/10.1002/2014jg002703

Schiecke, K., Pester, B., Feucht, M., Leistritz, L., & Witte, H. (2015). Convergent cross mapping: Basic concept, influence of estimation parameters and practical application. In *2015 37th annual international conference of the IEEE engineering in medicine and biology society (EMBC)* (pp. 7418–7421).

Seyednasrollah, B., Young, A. M., Hufkens, K., Milliman, T., Friedl, M. A., Frolking, S., et al. (2019). PhenoCam dataset v2.0: Vegetation phenology from digital camera imagery, 2000-2018 [Dataset]. ORNL DAAC. https://doi.org/10.3334/ORNLDAAC/1674

Seyfferth, A. L., Bothfeld, F., Vargas, R., Stuckey, J. W., Wang, J., Kearns, K., et al. (2020). Spatial and temporal heterogeneity of geochemical controls on carbon cycling in a tidal salt marsh. *Geochimica et Cosmochimica Acta*, *282*, 1–18. https://doi.org/10.1016/j.gca.2020.05.013

Stavert, A. R., Saunois, M., Canadell, J. G., Poulter, B., Jackson, R. B., Regnier, P., et al. (2022). Regional trends and drivers of the global methane budget. *Global Change Biology*, *28*(1), 182–200. https://doi.org/10.1111/gcb.15901

Strom, L., Falk, J. M., Skov, K., Jackowicz-Korczynski, M., Mastepanov, M., Christensen, T. R., et al. (2015). Controls of spatial and temporal variability in CH4 flux in a high arctic fen over three years. *Biogeochemistry*, *125*(1), 21–35. https://doi.org/10.1007/s10533-015-0109-0

Sturtevant, C., Ruddell, B. L., Knox, S. H., Verfaillie, J., Matthes, J. H., Oikawa, P. Y., & Baldocchi, D. (2016). Identifying scale-emergent, nonlinear, asynchronous processes of wetland methane exchange. *Journal of Geophysical Research: Biogeosciences*, *121*(1), 188–204. https://doi.org/10.1002/2015jg003054

Sugihara, G. (1994). Nonlinear forecasting for the classification of natural time series philosophical transactions of the Royal Society of London. *Series A: Physical and Engineering Sciences*, *348*, 477–495. https://doi.org/10.1098/rsta.1994.0106

Sugihara, G., May, R., Ye, H., Hsieh, C.-H., Deyle, E., Fogarty, M., & Munch, S. (2012). Detecting causality in complex ecosystems. *Science*, *338*(6106), 496–500. https://doi.org/10.1126/science.1227079

Sugihara, G., & May, R. M. (1990). Nonlinear forecasting as a way of distinguishing chaos from measurement error in time series. *Nature*, *344*(6268), 734–741. https://doi.org/10.1038/344734a0

Sun, X., Fang, W., Gao, X., An, S., Liu, S., & Wu, T. (2021). Time-varying causality inference of different nickel markets based on the convergent cross mapping method. *Resources Policy*, *74*, 102385. https://doi.org/10.1016/j.resourpol.2021.102385

Tokida, T., Miyazaki, T., Mizoguchi, M., Nagata, O., Takakai, F., Kagemoto, A., & Hatano, R. (2007). Falling atmospheric pressure as a trigger for methane ebullition from peatland. *Global Biogeochemical Cycles*, *21*(2), GB2003. https://doi.org/10.1029/2006gb002790

Trifunovic, B., Vazquez-Lule, A., Capooci, M., Seyfferth, A. L., Moffat, C., & Vargas, R. (2020). Carbon dioxide and methane emissions from temperate salt marsh tidal creek. *Journal of Geophysical Research: Biogeosciences*, *125*(8), e2019JG005558. https://doi.org/10.1029/2019jg005558

Tsonis, A. A., Deyle, E. R., Ye, H., & Sugihara, G. (2018). Convergent cross mapping: Theory and an example. In A. A. Tsonis (Ed.), *Advances in nonlinear geosciences* (pp. 587–600). Springer International Publishing.

Turner, J., Desai, A. R., Thom, J., & Wickland, K. P. (2021). Lagged wetland CH_4 flux response in a historically wet year. *Journal of Geophysical Research: Biogeosciences*, *126*(11), e2021JG006458. https://doi.org/10.1029/2021jg006458

Ushio, M., & Kawatsu, K. (2020). Forecasting ecological time series using empirical dynamic modeling: A tutorial for simplex projection and S-map. In A. Mougi (Ed.), *Diversity of functional traits and interactions: Perspectives on community dynamics* (pp. 193–213). Springer Singapore.

Vargas, R. (2020). AmeriFlux BASE US-StJ St Jones reserve, ver. 2-5 [Dataset]. AmeriFlux AMP. https://doi.org/10.17190/AMF/1480316

Vargas, R., Detto, M., Baldocchi, D. D., & Allen, M. F. (2010). Multiscale analysis of temporal variability of soil CO_2 production as influenced by weather and vegetation. *Global Change Biology*, *16*(5), 1589–1605. https://doi.org/10.1111/j.1365-2486.2009.02111.x

Vargas, R., & Le, V. H. (2023). The paradox of assessing greenhouse gases from soils for nature-based solutions. *Biogeosciences*, *20*(1), 15–26. https://doi.org/10.5194/bg-20-15-2023

Vargas, R., Sánchez-Cañete, P., Serrano-Ortiz, P., Curiel Yuste, J., Domingo, F., López-Ballesteros, A., & Oyonarte, C. (2018). Hot-moments of soil CO_2 efflux in a water-limited grassland. *Soil Systems*, *2*(3), 47. https://doi.org/10.3390/soilsystems2030047

Vázquez-Lule, A., Seyfferth, A. L., Limmer, M. A., Mey, P., Guevara, M., & Vargas, R. (2022). Hyperspectral reflectance for measuring canopy-level nutrients and photosynthesis in a salt marsh. *Journal of Geophysical Research: Biogeosciences*, *127*(11), e2022JG007088. https://doi.org/10.1029/2022jg007088

Vázquez-Lule, A., & Vargas, R. (2021). Biophysical drivers of net ecosystem and methane exchange across phenological phases in a tidal salt marsh. *Agricultural and Forest Meteorology*, *300*, 108309. https://doi.org/10.1016/j.agrformet.2020.108309

Vázquez-Lule, A., & Vargas, R. (2023). Proximal remote sensing and gross primary productivity in a temperate salt marsh. *Agricultural and Forest Meteorology*, *341*, 109639. https://doi.org/10.1016/j.agrformet.2023.109639

Wang, Y., Yang, J., Chen, Y., De Maeyer, P., Li, Z., & Duan, W. (2018). Detecting the causal effect of soil moisture on precipitation using convergent cross mapping. *Scientific Reports*, *8*(1), 12171. https://doi.org/10.1038/s41598-018-30669-2

Wang, Z. P., & Han, X. G. (2005). Diurnal variation in methane emissions in relation to plants and environmental variables in the Inner Mongolia marshes. *Atmospheric Environment*, *39*(34), 6295–6305. https://doi.org/10.1016/j.atmosenv.2005.07.010

Wuebbles, D. J., & Hayhoe, K. (2002). Atmospheric methane and global change. *Earth-Science Reviews*, *57*(3–4), 177–210. https://doi.org/10.1016/s0012-8252(01)00062-9

Wutzler, T., Lucas-Moffat, A., Migliavacca, M., Knauer, J., Sickel, K., Šigut, L., et al. (2018). Basic and extensible post-processing of eddy covariance flux data with REddyProc. *Biogeosciences*, *15*(16), 5015–5030. https://doi.org/10.5194/bg-15-5015-2018

Yang, B., Li, X., Lin, S., Jiang, C., Xue, L., Wang, J., et al. (2021). Invasive *Spartina alterniflora* changes the Yangtze Estuary salt marsh from CH4 sink to source. *Estuarine, Coastal and Shelf Science*, *252*, 107258. https://doi.org/10.1016/j.ecss.2021.107258

Ye, A., Clark, E. D., & Sugihara, G. (2016). rEDM: an R package for empirical dynamic modeling and convergent cross-mapping. Retrieved from cran.r-project.org

Ye, H., Deyle, E. R., Gilarranz, L. J., & Sugihara, G. (2015). Distinguishing time-delayed causal interactions using convergent cross mapping. *Scientific Reports*, *5*(1), 14750. https://doi.org/10.1038/srep14750

Yuan, J. J., Ding, W. X., Liu, D. Y., Kang, H., Xiang, J., & Lin, Y. X. (2016). Shifts in methanogen community structure and function across a coastal marsh transect: Effects of exotic *Spartina alterniflora* invasion. *Scientific Reports*, *6*(1), 18777. https://doi.org/10.1038/srep18777

Yvon-Durocher, G., Allen, A. P., Bastviken, D., Conrad, R., Gudasz, C., St-Pierre, A., et al. (2014). Methane fluxes show consistent temperature dependence across microbial to ecosystem scales. *Nature*, *507*(7493), 488–491. https://doi.org/10.1038/nature13164

Zaki, M. T., & Abdul-Aziz, O. I. (2022). Predicting greenhouse gas fluxes in coastal salt marshes using artificial neural networks. *Wetlands*, *42*(5), 37. https://doi.org/10.1007/s13157-022-01558-2

Zhang, Q., Ting-Ting, L., Zhang, Q., Guo-Cheng, W., Li-Jun, Y., Bin, G., & Peng-Fei, H. (2020). Accuracy analysis in CH4MODwetland in the simulation of CH_4 emissions from Chinese wetlands. *Advances in Climate Change Research*, *11*(1), 52–59. https://doi.org/10.1016/j.accre.2020.06.003

Zhang, Y. H., & Ding, W. X. (2011). Diel methane emissions in stands of *Spartina alterniflora* and Suaeda salsa from a coastal salt marsh. *Aquatic Botany*, *95*(4), 262–267. https://doi.org/10.1016/j.aquabot.2011.08.005

Zhang, Z., Zimmermann, N. E., Stenke, A., Li, X., Hodson, E. L., Zhu, G. F., et al. (2017). Emerging role of wetland methane emissions in driving 21st century climate change. *Proceedings of the National Academy of Sciences of the United States of America*, *114*(36), 9647–9652. https://doi.org/10.1073/pnas.1618765114

Zhu, X. D., Meng, L. X., Zhang, Y. H., Weng, Q. H., & Morris, J. (2019). Tidal and meteorological influences on the growth of invasive *Spartina alterniflora*: Evidence from UAV Remote Sensing. *Remote Sensing*, *11*(10), 1208. https://doi.org/10.3390/rs11101208

Zhu, X. D., Zhuang, Q. L., Qin, Z. C., Glagolev, M., & Song, L. L. (2013). Estimating wetland methane emissions from the northern high latitudes from 1990 to 2009 using artificial neural networks. *Global Biogeochemical Cycles*, *27*(2), 592–604. https://doi.org/10.1002/gbc.20052